AERODYNAMIC DESIGN VIA OPTIMIZATION

Ki D. Lee* and Sinan Eyi**
Aeronautical and Astronautical Engineering
University of Illinois
Urbana, Illinois, U. S. A.

Abstract

An aerodynamic design optimization method is presented which generates an airfoil producing a specified surface pressure distribution at a transonic speed. The design procedure is based on the coupled Euler and boundary layer technology in order to include the rotational viscous physics which characterizes transonic flows. A least-square optimization technique is used to minimize pressure discrepancies between the target and designed airfoils. The method is demonstrated with several examples at transonic speeds. The design optimization process converges quickly, which makes the method attractive for practical engineering applications.

I. Introduction

In recent years, computational fluid dynamics (CFD) has become a valuable engineering tool in the aircraft industry. CFD plays a complementary role, not a replacement, to experiments in practical design communities. Rubbert [1] showed some good examples of the use of CFD and experiment in combination for transonic design. A major strength of CFD is the ability to produce detailed insights into complex flow phenomena. The process of decomposition and parameterization can help identify the cause of weak aerodynamic performance, and the microscopic understanding of the flow can lead to improved design. Continuing advances in computer hardware and simulation techniques provide an unprecedented opportunity for CFD. Now simulations of more complete configurations with more complex physics can be performed at an affordable cost. Accuracy and reliability of the computation have been continuously improved. The use of high-level flow models and large-size refined grids enables one to analyze flows with complicated structures and various length scales. Compared to the remarkable advances in analysis capability, however, relatively few advances have been made in design technology. Conventional design practices, therefore, often depend on analysis methods through iterative cut-and-try approaches.

A unique advantage of CFD is the capability of inverse design. Inverse design determines directly the airfoil geometry which produces the pressure distribution specified by a designer. Many existing inverse design methods are based on the potential flow assumption due to its simplicity. Volpe and Melnik [2] employed an inverse design method using the nonlinear full potential formulation. Bauer and colleagues [3] used the hodograph method which solves the full potential equation in the hodograph plane where the equations are linear. The potential flow model, however, cannot properly represent transonic features such as embedded shock waves and shock-boundary layer interactions. An accurate analytic capability is a prerequisite for a successful design because the quality of the design depends on the quality of the method used to predict the flow field. Several inverse design methods were demonstrated using the Euler formulations by Giles and Drela [4] and Mani [5]. Design methods based on the Navier-Stokes equations are still regarded impractical and too expensive.

Instead of achieving the prescribed pressure distribution, some design methods use a constrained optimization process to improve design by minimizing some design constraints such as drag. Examples of this method were presented by Hicks, et al [6], Vanderplaats [7], and Chen and Chow [8]; all of those were based on the full potential formulation. Recently, Jameson [9] developed a design optimization process using control theory and conformal mapping based on the potential and Euler equations. The constrained design approaches eliminate the difficulty in furnishing a proper target pressure distribution but have a disadvantage due to relatively high costs in obtaining converged results.

The present method is an inverse design optimization procedure using the coupled Euler and boundary layer technology. The airfoil geometry is modified through a least-square optimization process to produce a specified pressure distribution, starting from an initial baseline configuration. The method includes the rotational viscous physics which is significant at supercritical transonic speeds. The method is an extension of the author's earlier effort which is based on the inviscid Euler formulation [10]. A merit of the present method is that the optimization cycle converges quickly so that the process is affordable even with the use of high-level physics. In this paper, the base technologies of flow analysis used in the design process will be discussed first, followed by the description of the optimization algorithm. The design method is tested for several transonic airfoils at both subcritical and supercritical flow conditions.

II. Euler - Boundary Layer Coupling

The reliability of a design method depends on the ability to produce accurate flow solutions. A design result is not useful if the flow code used is not reliable. Although the Navier-Stokes equations are attractive, present-day Navier-Stokes technologies are not yet mature enough to be reliable or versatile. The flow analysis technology used in the present design process is based on the Euler equations coupled with the boundary layer equations. The Euler equations can model the rotational flow physics such as embedded shock waves in transonic flows and the boundary layer equations serve as boundary conditions along the airfoil surface and the wake. A simultaneous

* Associate Professor
** Graduate Research Assistant

coupling approach is adopted which solves the unsteady Euler equations and the unsteady integral boundary layer equations at the same time. Steady-state solutions are achieved as a time asymptote. The simultaneous coupling has been shown to be an efficient means of inviscid-viscous coupling for a wide range of transonic analyses [11]. The simultaneous coupling is especially beneficial in the design process since it can include the boundary layer effects without involving an extra periodic coupling.

The two-dimensional unsteady Euler equations are:

$$\frac{\partial w}{\partial t}+\frac{\partial f}{\partial x}+\frac{\partial g}{\partial y}=0 \qquad (1)$$

where

$$w=\begin{Bmatrix}\rho\\ \rho u\\ \rho v\\ \rho E\end{Bmatrix} \quad f=\begin{Bmatrix}\rho u\\ \rho u^2+p\\ \rho uv\\ \rho uH\end{Bmatrix} \quad g=\begin{Bmatrix}\rho v\\ \rho vu\\ \rho v^2+p\\ \rho vH\end{Bmatrix}$$

In the equation, ρ, p, u, v, E, and H are the density, pressure, velocity components in the x and y directions, total energy, and total enthalpy respectively. A surface fitted coordinate system is used to facilitate the implementation of the surface boundary conditions. Equation (1) is then transformed from the physical space (x, y) into the computational domain (ξ, η) :

$$\frac{\partial W}{\partial t}+\frac{\partial F}{\partial \xi}+\frac{\partial G}{\partial \eta}=0 \qquad (2)$$

where $W = wh$

$F = fy_\eta - gx_\eta$

$G = gx_\xi - fy_\xi$

and $h = x_\xi y_\eta - x_\eta y_\xi$.

In Equation (2), x_ξ, y_ξ, x_η, and y_η are the transformation metrics and h is the Jacobian of the transformation.

The finite volume method is adopted for the spatial discretization and the equation is integrated in conservative form to ensure conservation of flow quantities. Flow variables are defined at the cell center and centered differencing is used for the spatial derivatives. Artificial viscosity terms are added to enforce numerical stability. Integration in the time domain is performed explicitly using a fourth-order Runge-Kutta scheme. Since time accuracy is not sought, local time steps are used to accelerate convergence.

Grids with a C-mesh topology are used. Characteristic boundary conditions are imposed at the far field boundary based on the one-dimensional eigenvalue analysis. In the inviscid Euler analysis, the boundary condition on the configuration surface is the impermeable condition, which implies zero normal mass flux across the surface. During the iterative design cycle, however, the surface geometry keeps changing and new computational grids are required to accommodate the changes. Another way of implementing the geometry changes is the use of a transpiration boundary condition, given by

$$\rho q_n = \frac{d}{ds}[\rho q_t(\Delta y + \delta^*)] \qquad (3)$$

where q_n and q_t are the normal and tangential components of the surface velocity respectively. s is the distance along the airfoil surface. Δy is the change of the airfoil geometry from the baseline airfoil and δ^* is the displacement thickness of the boundary layer. The total transpiration mass flux at the airfoil surface is attributed to both the boundary layer displacement and the design update. In the Euler formulation, the transpiration mass flux also contributes to the momentum and energy fluxes. Non-zero transpiration fluxes are also allowed along the wake to account for the boundary layer effects.

In the boundary layer formulation, the viscous effects are assumed to be confined in the thin boundary layer along the surface and wake. The boundary layer calculations are performed by solving the following integral form of the momentum and kinetic energy equations:

$$\frac{\partial}{\partial t}(\rho_e u_e \delta^*) - u_e \frac{\partial}{\partial t}(\rho_e \theta_\rho) + \frac{\partial}{\partial x}(\rho_e u_e^2 \theta) + \rho_e u_e \delta^* \frac{\partial u_e}{\partial x} = \tau_w \qquad (4)$$

$$\frac{\partial}{\partial t}[\rho_e u_e^2(\theta + \delta^* - \theta_\rho)] + \rho_e(\theta_\rho - \delta_u^*)\frac{\partial u_e^2}{\partial t} + \frac{\partial}{\partial x}(\rho_e u_e^3 \theta^*) + \rho_e u_e(\delta^* - \delta_u^*)\frac{\partial u_e^2}{\partial x} = \tau_w u_e D_E$$

where

$$\delta^* = \int_0^\infty \left(1 - \frac{\rho u}{\rho_e u_e}\right) dy \qquad \text{(displacement thickness)}$$

$$\theta = \int_0^\infty \frac{\rho u}{\rho_e u_e}\left(1 - \frac{u}{u_e}\right) dy \qquad \text{(momentum thickness)}$$

$$\theta^* = \int_0^\infty \frac{\rho u}{\rho_e u_e}\left(1 - \frac{u^2}{u_e^2}\right) dy \qquad \text{(kinetic energy thickness)}$$

$$\delta_u^* = \int_0^\infty \left(1 - \frac{u}{u_e}\right) dy \qquad \text{(velocity thickness)}$$

$$\theta_\rho = \int_0^\infty \left(1 - \frac{\rho}{\rho_e}\right) dy \qquad \text{(density thickness)}$$

and

$$D_E = \int_0^\infty \frac{\tau}{\tau_w}\frac{\partial}{\partial y}\left(\frac{u}{u_e}\right) dy \qquad \text{(dissipation integral)}$$

In the above boundary layer equations, (x, y) and (u, v) are coordinates and velocity components in the streamwise and transverse directions respectively. The subscripts e and w stand for the values at the boundary layer edge and the wall respectively. τ is the shear stress due to viscosity. The unsteady boundary layer equations are marched in time

using the same fourth-order Runge-Kutta scheme as in the Euler integration. The Equation (4) is rewritten in the following form of a linear system:

$$\frac{\partial}{\partial t}\begin{Bmatrix}\theta\\ \overline{H}\end{Bmatrix} + u_e[C]\frac{\partial}{\partial x}\begin{Bmatrix}\theta\\ \overline{H}\end{Bmatrix} = \begin{Bmatrix}R1\\ R2\end{Bmatrix} \qquad (5)$$

where $\overline{H}$ is the kinematic shape parameter, which is defined as a function

$$\overline{H} = \overline{H}(H, M_e) \qquad (6)$$

where H is the shape factor defined by the ratio δ^* over θ and M_e is the Mach number at the boundary layer edge. The right hand side terms $R1$ and $R2$ and the coefficient matrix $[C]$ in Equation (5) are also functions of the inviscid edge condition and various shape factors which are given by proper closure conditions. Empirically defined closure conditions are adopted for both laminar and turbulent flows [11]. The transition point is either fixed or predicted based on Orr-Sommerfield spatial amplification theory. Time steps for integrating the boundary layer equations are determined from the eigenvalues of the coefficient matrix of Equation (5) to satisfy the von Neumann stability criterion. The boundary layer calculations are extended into the wake with zero skin friction.

III. Design Optimization

The design goal in the present study is to obtain the airfoil geometry which produces a specified pressure distribution, known as the target pressure distribution, at a specified flight condition. Other constraints, such as minimum drag, can be imposed as a design goal. The design process starts with a guess for the target airfoil geometry, namely an initial baseline airfoil. Flow analysis of the baseline airfoil examines the quality of the guess. Using an initial airfoil with the pressure distribution that is already close to the target pressure distribution would speed up the design process. Any analysis code can be used to obtain flow solutions, but a more accurate analysis capability will produce a more reliable design.

A successful design process implies an automatic and systematic procedure for improving the guess. The airfoil geometry is updated by perturbing the initial airfoil geometry. The perturbation is defined as a linear combination of base functions which are prescribed as smoothly distributed curves over the airfoil chord. A flow analysis code is used to obtain the variation in the pressure distribution due to each small perturbation. For consistency, the same code is used in both the analysis and variation steps. The variation is a measure of the response of the flow field to each small geometry perturbation. A least-square optimization technique then determines the magnitude of each perturbation needed to achieve the target pressure distribution. This procedure is repeated iteratively. Figure 1 illustrates the whole design process.

The geometry perturbation Δy is defined as a linear combination of the following base functions f_k:

$$\Delta y(x) = \sum_{k=1}^{K} \delta_k f_k(x) \qquad (7)$$

where x is the normalized chordwise position on the airfoil and K stands for the number of base functions to be used.

The weighting coefficients δ_k in the equation are to be determined through the optimization procedure. A base function is a smooth curve that represents an added perturbation on the airfoil surface. In the present study, the base functions are composed of two patched polynomials:

$$f_k(x) = 1 - \left(\frac{x_k - x}{x_k}\right)^2 \left(1 + \frac{A}{(1-x_k)^2}\left(\frac{x}{x_k}\right)\right) \quad \text{for } 0 < x \le x_k \qquad (8)$$

$$f_k(x) = 1 - \left(\frac{x - x_k}{1 - x_k}\right)^2 \left(1 + \frac{B}{(x_k)^2}\left(\frac{1-x}{1-x_k}\right)\right) \quad \text{for } x_k < x \le 1$$

where $A = \max(0, 1 - 2x_k)$

and $B = \max(0, 2x_k - 1)$.

The polynomials join smoothly at coordinate x_k where the perturbation is maximum. In Equation (8), a parabola on one side of x_k is patched with a cubic on the other side. This provides continuities up to second order derivatives without oscillation. Figure 2 shows examples of the base functions with x_k at 0.05, 0.1, 0.2, 0.3, 0.5, 0.7, and 0.9. A total of fourteen base functions were used; seven on both the upper and lower sides.

The accuracy and efficiency of a design process depends on the number of base functions. The performance also depends on the particular choice of base functions. The number and the shape of base functions may cause the resulting perturbations, and hence the pressure distributions, to be wavy. Therefore, a smoothing procedure is applied to prevent wavy surfaces after obtaining the perturbations. A least-square smoothing is applied by fitting the resulting perturbations into a smooth polynomial.

In order to judge the design quality and to monitor the convergence of the design cycle, a convergence parameter is defined. This parameter is based on the root-mean-square of length-weighted pressure discrepancies between the target pressure and the pressure of the designed airfoil:

$$CP = \left(\frac{\sum_{i=1}^{I} (P_{t_i} - P_{b_i})^2 \Delta S_i}{\sum_{i=1}^{I} \Delta S_i} \right)^{\frac{1}{2}} \qquad (9)$$

where P_{t_i} and P_{b_i} are the target and baseline pressures respectively on the airfoil surface at point i and ΔS_i is the length of the surface element. There are a total of I points on the airfoil surface.

The objective of the optimization procedure is to minimize the discrepancy given by the convergence parameter. A least-square method is chosen for the optimization procedure. The differences between the target and baseline pressures are to be reduced by adding perturbations to the baseline geometry to improve the guess iteratively. The object function to be minimized through the optimization is chosen as follows:

$$J = \sum_{i=1}^{I} \left(P_{t_i} - P_{b_i} - \sum_{k=1}^{K} \frac{\partial P_i}{\partial \delta_k} \delta_k \right)^2 \Delta S_i \qquad (10)$$

where $\partial P_i / \partial \delta_k$ is the response of the flow field to the small perturbation δ_k, which is to be determined in a least-square sense. Hence, the minimization condition yields, for $j = 1, K$

$$\frac{\partial J}{\partial \delta_j} = 0 = -2 \sum_{i=1}^{I} \left(P_{t_i} - P_{b_i} - \sum_{k=1}^{K} \frac{\partial P_i}{\partial \delta_k} \delta_k \right) \frac{\partial P_i}{\partial \delta_j} \Delta S_i \quad (11)$$

which can be rewritten, for $j = 1, K$

$$\sum_{k=1}^{K} \left(\sum_{i=1}^{I} \frac{\partial P_i}{\partial \delta_j} \frac{\partial P_i}{\partial \delta_k} \Delta S_i \right) \delta_k = \sum_{i=1}^{I} \frac{\partial P_i}{\partial \delta_j} (P_{t_i} - P_{b_i}) \Delta S_i \quad (12)$$

Equation (12) is then solved for the δ_k's that define the perturbations required to improve the guess.

A potential disadvantage of the inverse optimization method may be the relatively high cost of computation. With the trend of rapid reduction in computing cost, however, the approach can provide a more robust design tool than inverse design methods. An optimization can at least provide the most probable geometry for given constraints, although the requirement may not be fully satisfactory. It can avoid the so-called closure problem at the airfoil trailing edge, which has been an issue in conventional inverse design methods. Multiple constraints can be imposed together, and off-design performance can also be included as a part of the design requirements.

IV. Design Exercises

As discussed, the accuracy of the flow analysis determines the quality of the resulted design. Therefore the analysis method was first validated using several transonic test cases for the airfoil RAE-2822 by comparing with the experimental data in Reference 12. The flow analysis in the present design method is based on the Euler and boundary layer technology with a simultaneous coupling. The analysis was performed on a 129 x 33 grid of C-mesh topology with 76 points on the airfoil surface. Results for cases 6, 9, and 10 demonstrate a good agreement with experiment, as shown in Figures 3 to 5 respectively. The pressure distributions match well with the experimental results and shock positions are calculated accurately. Although no model was used for the shock-boundary layer interaction, in general good predictions were obtained for the boundary layer parameters except for Case 10. The experiment exhibits a flow separation for Case 10 at the front of the shock. The discrepancy between computed and measured boundary layer parameters increases substantially for Case 10, while still exhibiting good agreement in pressure distributions.

Next the design method was tested with the inviscid cases to evaluate its efficiency and performance at transonic speeds. Tests were performed using the NACA-0012 airfoil as the initial baseline airfoil and the RAE-2822 airfoil as the target airfoil. The mesh size used in the design practice is 97 x 20 with 61 points on the airfoil surface. The iteration in the time marching of the Euler equations was terminated when the maximum residual was reduced four orders of magnitude. Figures 6 and 7 exhibit the evolution of surface pressure distributions, designed airfoil geometry, and the convergence history for two transonic cases; one subcritical and the other supercritical. The convergence of the design cycle was measured by the convergence parameter defined in Equation (9). A typical design cycle requires about three times more computer time than one analysis cycle. Most of the time increase is contributed to the variation process of finding flow field responses to the perturbations. It can be seen, however, that the design process converges quickly, requiring usually less than six iterations for engineering accuracy.

The inverse design optimization procedure was then tested with the viscous calculations. The design cycle was initiated with inviscid design and switched to viscous design after three cycles, since the boundary layer calculation is sensitive to sudden geometry changes. Throughout the design cycle, the transition point was fixed at the three percent chord position in order to ensure numerical stability. The use of viscous physics did not alter the performance of the design method for Cases 3, 6, and 9 significantly, as shown in Figures 8 to 10. Excellent results were obtained in about six iteration cycles. However, the design cycle failed to give a converged design for Case 10 which contains a shock induced flow separation.

As discussed earlier, the performance of the method depends on the number and the shape of the base functions. Fewer than four base functions on each side were not satisfactory and more than seven each side did not improve the performance considering the increased cost. Base functions based on patched trigonometric functions were also tried but no remarkable differences were observed. The design performance is dependent on the initial guess but is not sensitive to the flow conditions unless strong flow separations are present in the flow field. The efficiency of the design optimization also depends on design constraints and the choice of the object function.

V. Conclusions

The developed design method has demonstrated to be an efficient design tool for transonic airfoils. It is based on the rotational Euler physics with the viscous coupling using the integral boundary layer formulation and hence it provides a good correlation with experiment at wide range of transonic speeds. The least-square optimization technique was proved efficient in designing the airfoil geometry subject to a specified pressure distribution. Fast convergence was experienced in most design practices at transonic speeds. Experiments with several design examples show that the method can be used as a practical design tool. The design procedure can be incorporated with other optimization techniques and/or different flow solvers. The method can also be extended into the constrained design optimization such as drag minimization. Further reduction of the design cost will make the method more attractive.

Acknowledgement

Computations for this work were performed on the Cray 2 computer provided by the National Center for Supercomputing Apllications at the University of Illinois.

References

1. Rubbert, P.E., "Use of CFD and Experiment in Transonic Aircraft Design," Symposium Transsonicum III, J. Zierep, H. Oertel (Eds.), Springer-Verlag, 1989, pp. 19-32.
2. Volpe, G. and Melnik, R.E., "The Design of Transonic Airfoils by a Well-Posed Inverse Method," International Conference on Inverse Design Concepts in Engineering Sciences, Austin, TX, October 1984.
3. Bauer, F., Garabedian, P., Korn, D., and Jameson, A., "Supercritical Wing Sections I, II, III," Lecture Notes in Economics and Mathematical Systems, Springer-Verlag, NY, 1972, 1975, 1977.
4. Giles, M.B. and Drela, M., "Two-Dimensional Transonic Aerodynamic Design Method", AIAA Journal, Vol. 25, No. 9, September 1987.
5. Mani, K.K., "Design Using Euler Equations", AIAA Paper 84-2166, AIAA 2nd Applied Aerodynamic Conference, Seattle, WA, August 1984.
6. Hicks, R.M., Murman, E.M. and Vanderplaats, G.N., "An Assessment of Aerofoil Design by Numerical Optimization", NASA TM X-3092, 1974.
7. Vanderplaats, G.N., "Efficient Algorithm for Numerical Airfoil Optimization," AIAA J. Aircraft, Vol. 16, No. 12, Dec. 1979, pp. 842-847.
8. Chen, M.-S. and Chow, C.-Y., " Numerical Optimization Design of Transonic Airfoils," Numerical Methods in Laminar and Turbulent Flow, Vol. 6, Part 1, Pineridge Press, 1989, pp. 905-915.
9. Jameson, A., "Aerodynamic Theory Via Control Theory," NASA CR 181749, ICASE Report 88-64, NASA Langley Research Center, 1988.
10. Lee, K.D. and Liu, P.H., " A Design Optimization Method Using the Euler Equations," Numerical Methods in Laminar and Turbulent Flow, Vol. 6, Part 1, Pineridge Press, 1989, pp. 773-782.
11. Eyi, S., "A Simultaneous Inviscid/Viscous Coupling Approach for Transonic Flows," M. S. Thesis, University of Illinois, Urbana, Illinois, 1989.
12. Cook, P.H., McDonald, M.A., and Firmin, M.C.P., "Aerofoil RAE 2822 - Pressure Distributions, and Boundary Layer and Wake Measurements," AGARD Advisory Report N0. 138, Paper A6, May 1979.

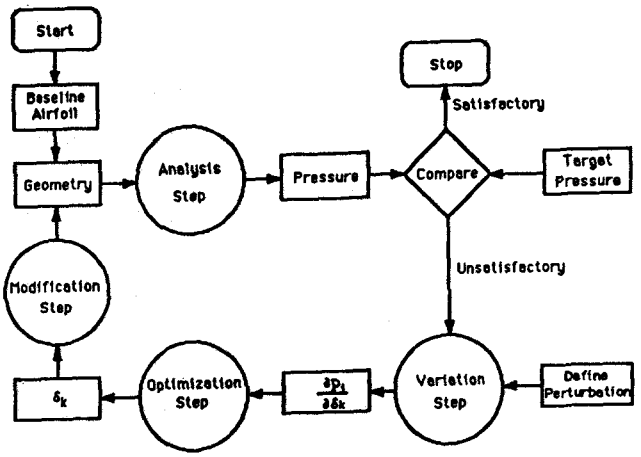

Figure 1. Design Procedure

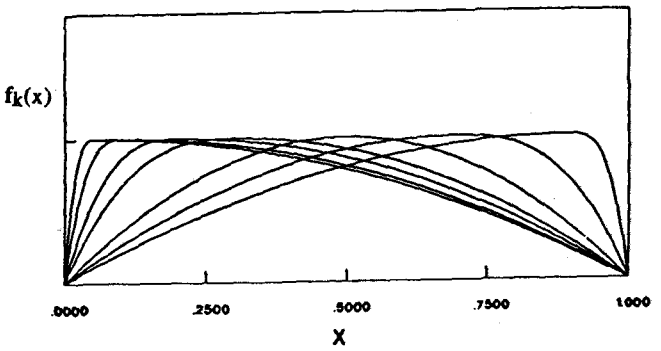

Figure 2. Examples of Base Functions

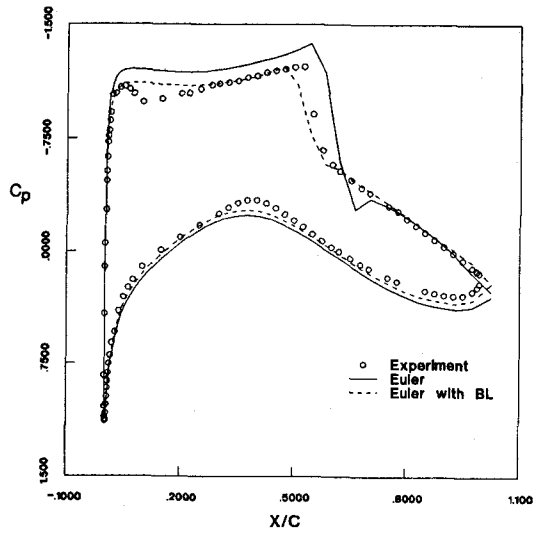

(a) Pressure distribution

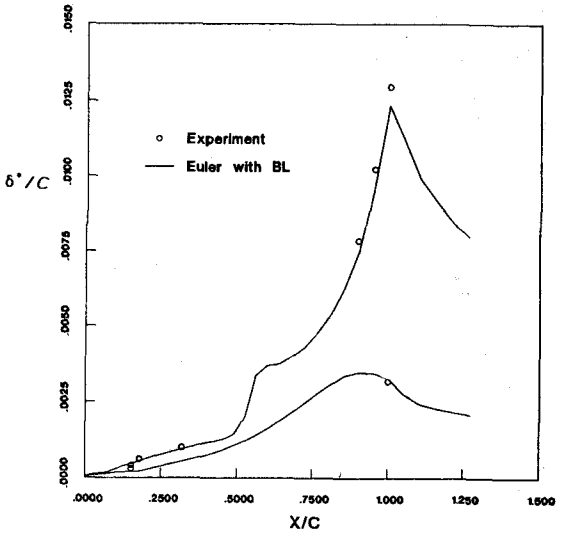

(b) Displacement thickness

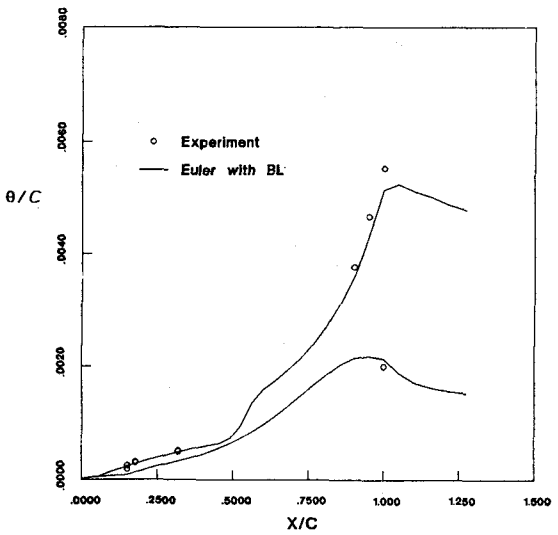

(c) Momentum thickness

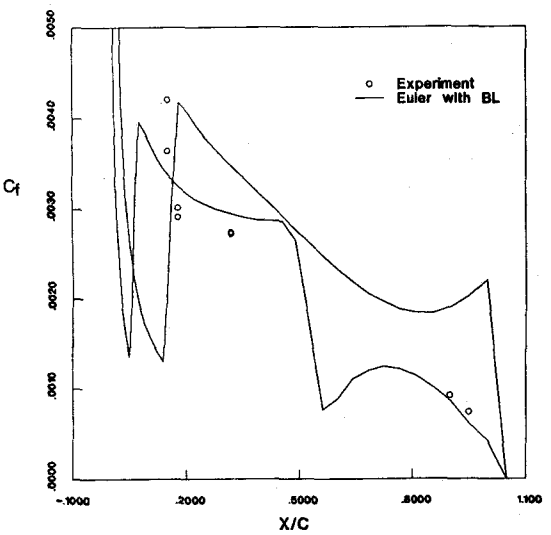

(d) Skin friction coefficient

Figure 3. Inviscid-Viscous Coupling: RAE 2822 Airfoil - Case 6
$M_\infty = 0.726$, $Re = 6.5 * 10^6$, $\alpha_g = 2.92^o$, $\alpha_c = 2.44^o$

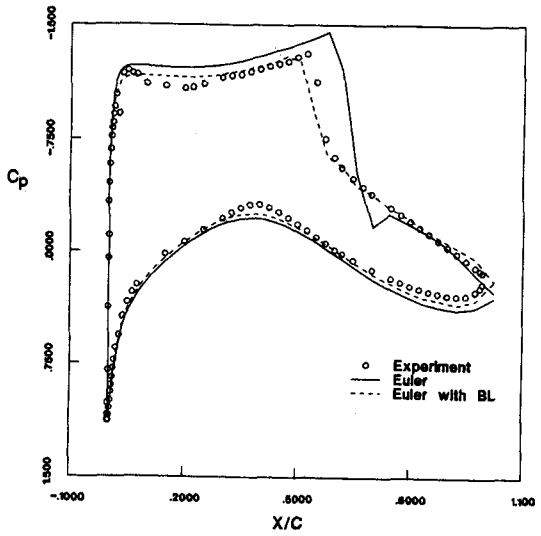

(a) Pressure distribution

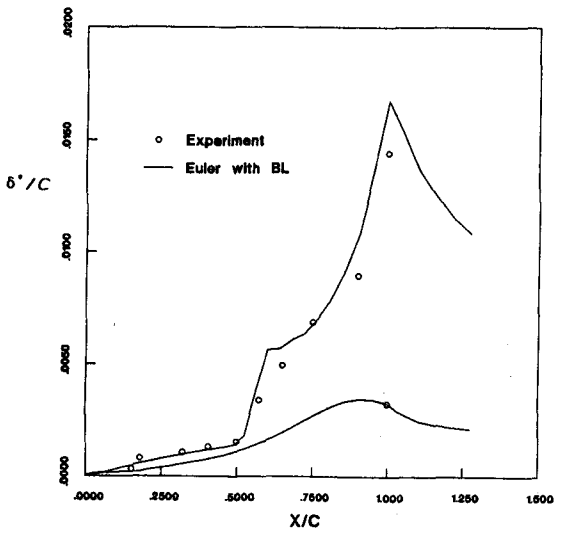

(b) Displacement thickness

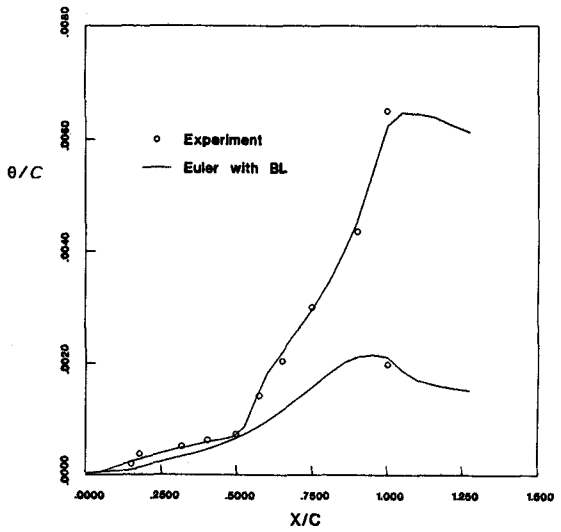

(c) Momentum thickness

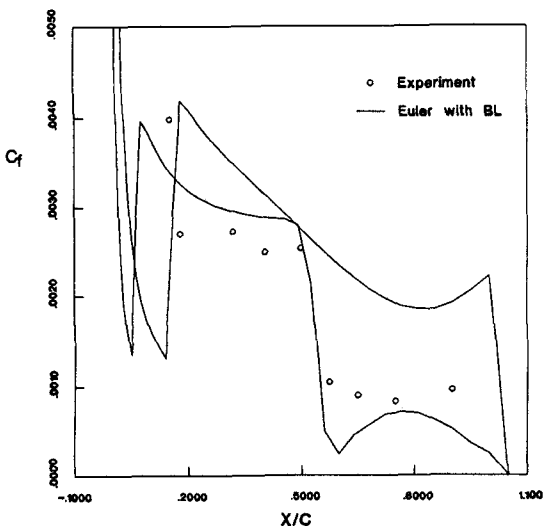

(d) Skin friction coefficient

Figure 4. Inviscid-Viscous Coupling: RAE 2822 Airfoil - Case 9
$M_\infty = 0.730$, $Re = 6.5 * 10^6$, $\alpha_g = 3.19°$, $\alpha_c = 2.78°$

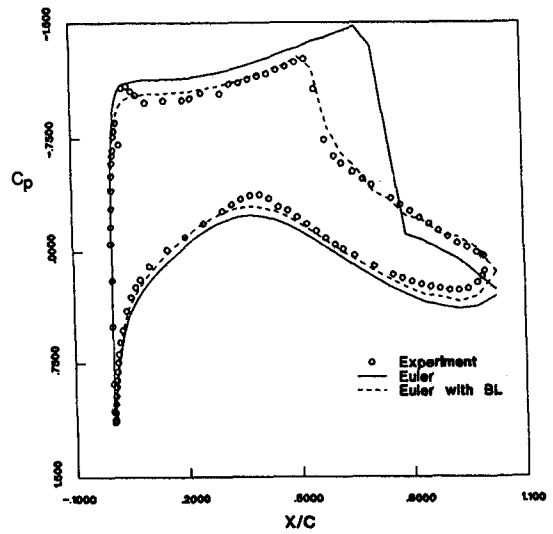

(a) Pressure distribution

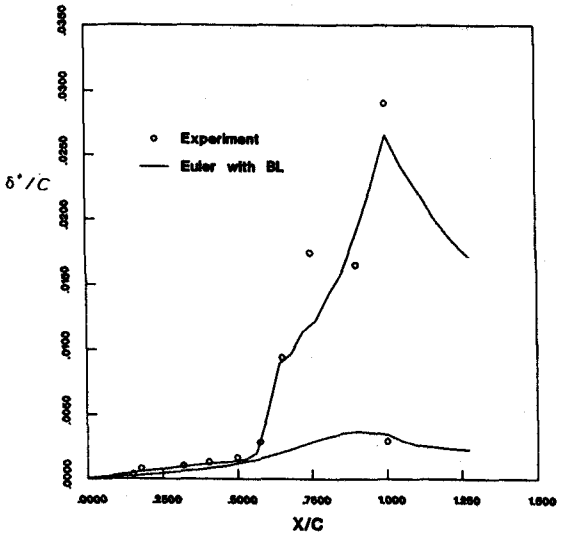

(b) Displacement thickness

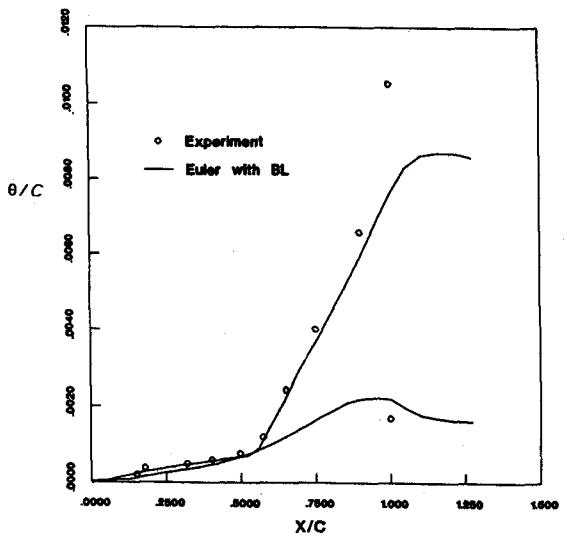

(c) Momentum thickness

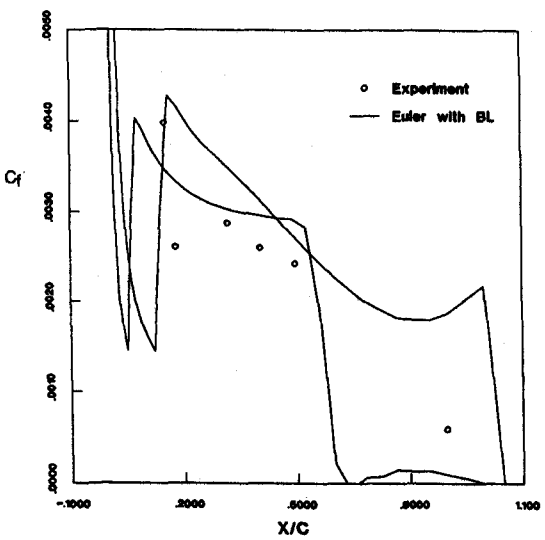

(d) Skin friction coefficient

Figure 5. Inviscid-Viscous Coupling: RAE 2822 Airfoil - Case 10
$M_\infty = 0.750$, $Re = 6.2 * 10^6$, $\alpha_g = 3.19°$, $\alpha_c = 2.70°$

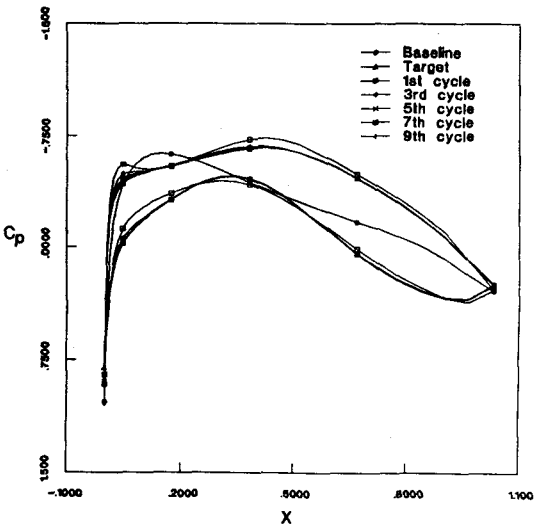

(a) Evolution of surface pressure

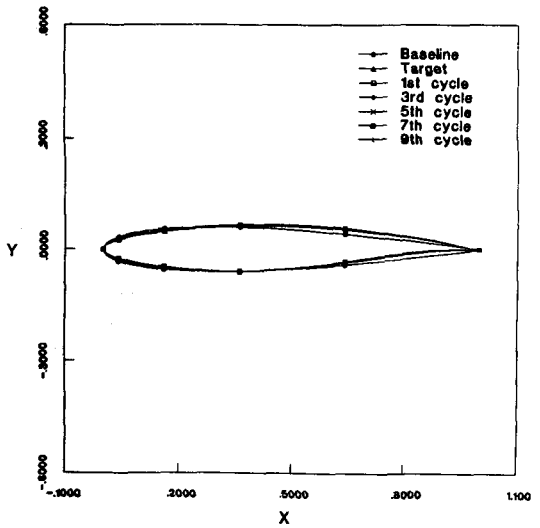

(b) Evolution of airfoil geometry

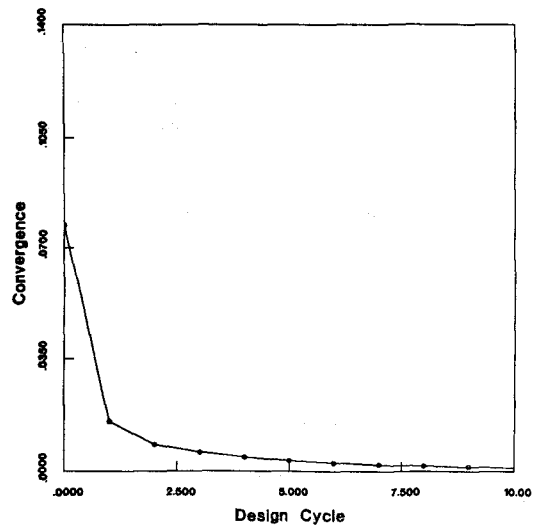

(c) Convergence history

Figure 6. Inviscid Design Practice: Subcritical From NACA 0012 to RAE 2822 Airfoil
$M_\infty = 0.70$, $\alpha_c = 0.0^\circ$

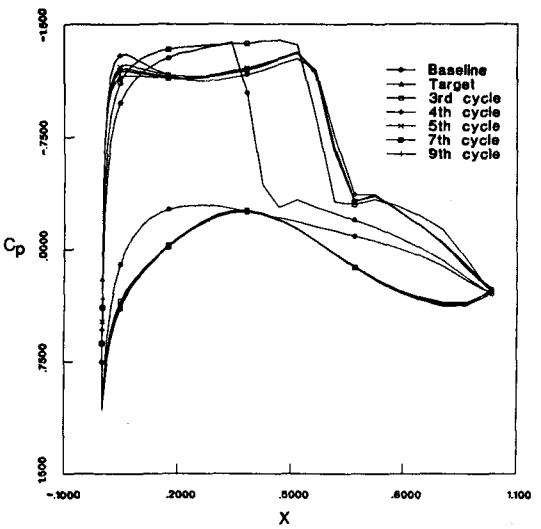

(a) Evolution of surface pressure

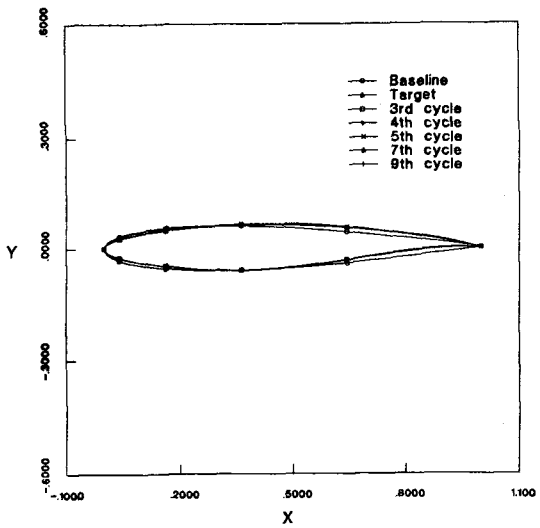

(b) Evolution of airfoil geometry

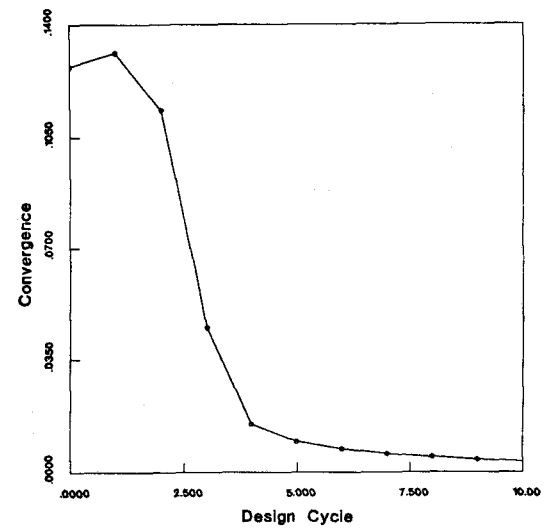

(c) Convergence history

Figure 7. Inviscid Design Practice: Supercritical From NACA 0012 to RAE 2822 Airfoil
$M_\infty = 0.726$, $\alpha_c = 2.44^\circ$

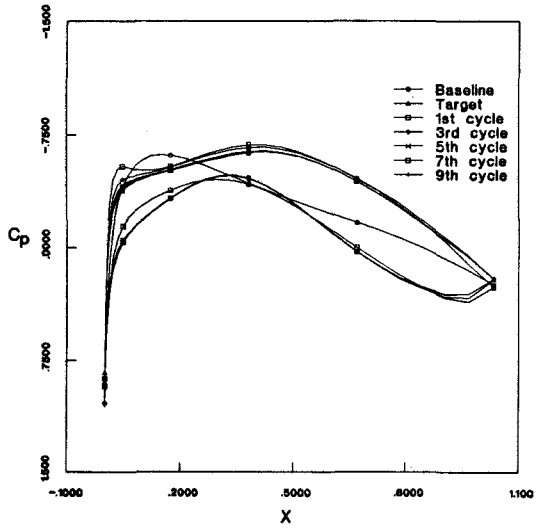

(a) Evolution of surface pressure

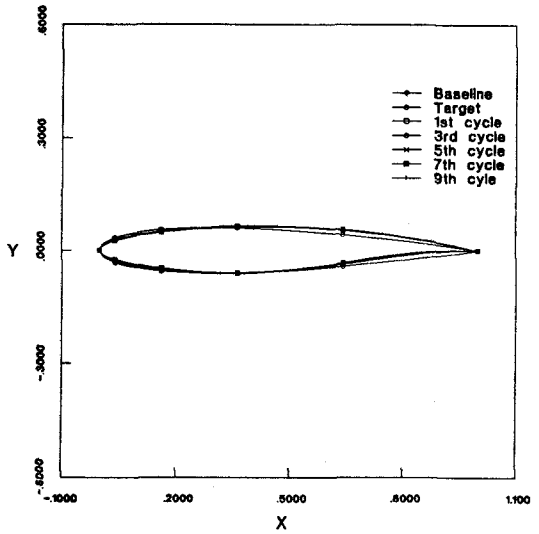

(b) Evolution of airfoil geometry

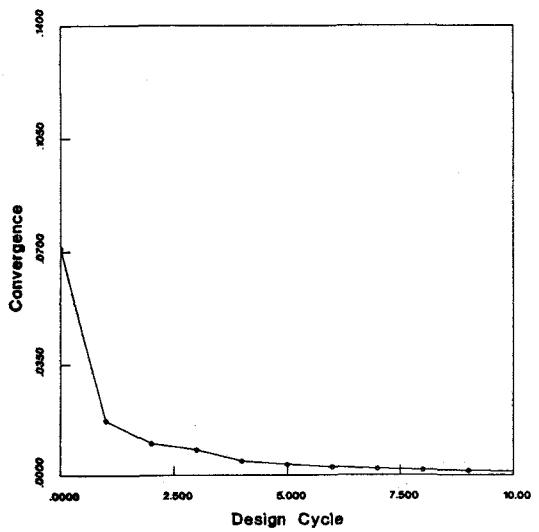

(c) Convergence history

Figure 8. Viscous Design Practice: Subcritical
From NACA 0012 to RAE 2822 Airfoil
$M_\infty = 0.70$, $Re = 6.5 * 10^6$, $\alpha_c = 0.0°$

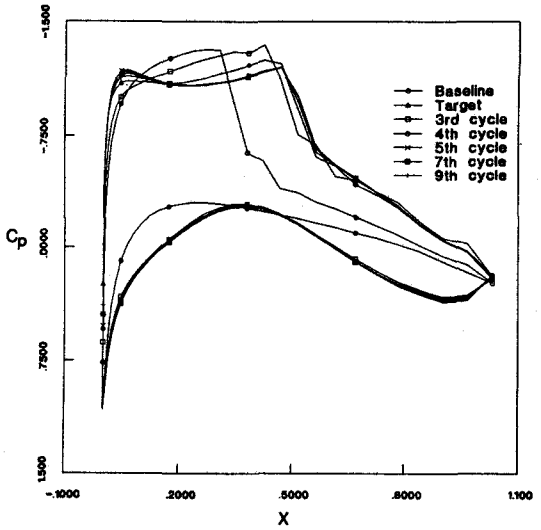

(a) Evolution of surface pressure

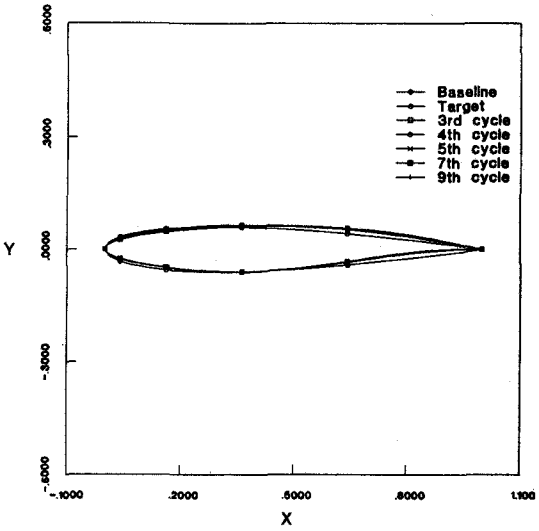

(b) Evolution of airfoil geometry

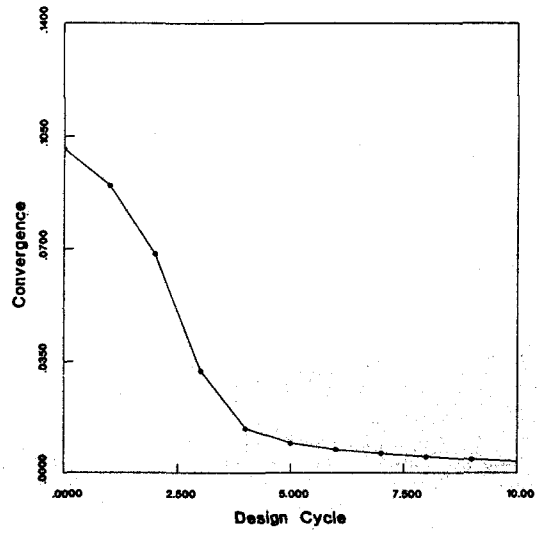

(c) Convergence history

Figure 9. Viscous Design Practice: Case 6
From NACA 0012 to RAE 2822 Airfoil
$M_\infty = 0.726$, $Re = 6.5 * 10^6$, $\alpha_c = 2.44°$

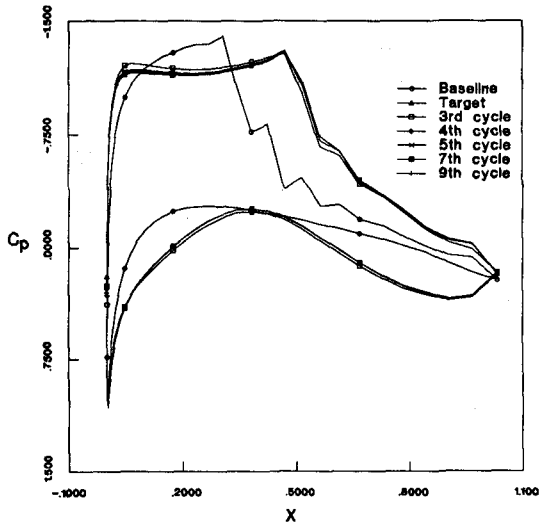

(a) Evolution of surface pressure

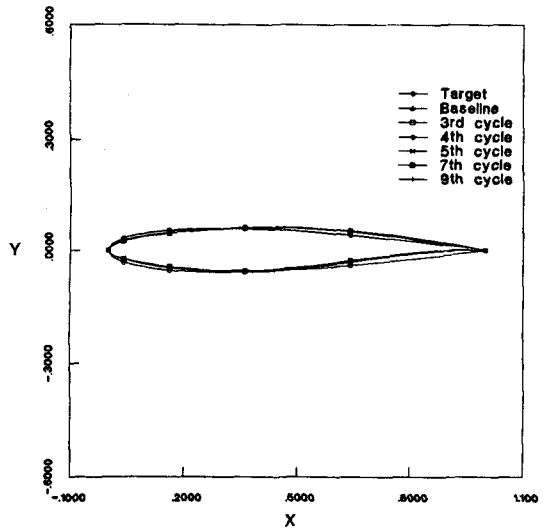

(b) Evolution of airfoil geometry

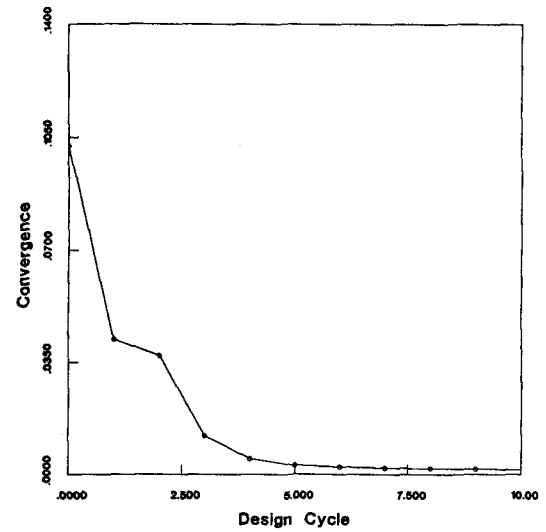

(c) Convergence history

Figure 10. Viscous Design Practice: Case 9
From NACA 0012 to RAE 2822 Airfoil
$M_\infty = 0.730$, $Re = 6.5 * 10^6$, $\alpha_c = 2.78^\circ$